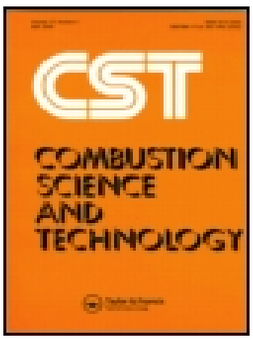

Taylor & Francis
Taylor & Francis Group

Combustion Science and Technology

ISSN: (Print) (Online) Journal homepage: https://www.tandfonline.com/loi/gcst20

Dual-comb Spectroscopy for Laminar Premixed Flames with a Free-running Fiber Laser

Ke Xu, Liuhao Ma, Jie Chen, Xin Zhao, Qiang Wang, Ruifeng Kan, Zheng Zheng & Wei Ren

To cite this article: Ke Xu, Liuhao Ma, Jie Chen, Xin Zhao, Qiang Wang, Ruifeng Kan, Zheng Zheng & Wei Ren (2021): Dual-comb Spectroscopy for Laminar Premixed Flames with a Free-running Fiber Laser, Combustion Science and Technology, DOI: 10.1080/00102202.2021.1879796

To link to this article: https://doi.org/10.1080/00102202.2021.1879796

COMBUSTION SCIENCE AND TECHNOLOGY
https://doi.org/10.1080/00102202.2021.1879796

Taylor & Francis
Taylor & Francis Group

ARTICLE

Dual-comb Spectroscopy for Laminar Premixed Flames with a Free-running Fiber Laser

Ke Xu[a], Liuhao Ma[a,b], Jie Chen[c], Xin Zhao[c], Qiang Wang[d], Ruifeng Kan[d], Zheng Zheng[c], and Wei Ren[a,b]

[a]Department of Mechanical and Automation Engineering, The Chinese University of Hong Kong, New Territories, Hong Kong SAR, China; [b]Shenzhen Research Institute, The Chinese University of Hong Kong, New Territories, Hong Kong SAR, China; [c]School of Electronic and Information Engineering, Beihang University, Beijing, China; [d]State Key Laboratory of Applied Optics, Changchun Institute of Optics, Fine Mechanics and Physics, Chinese Academy of Sciences, Changchun, China

ABSTRACT

Dual-comb spectroscopy (DCS) has emerged as an important new technique for high-resolution molecular spectroscopy. However, this powerful tool has not been widely utilized in combustion diagnostics due to the difficulty of maintaining the mutual coherence between the two comb sources. In this work, we demonstrated a free-running fiber-laser-based DCS for *in situ* and non-intrusive H_2O and C_2H_2 measurements in laminar premixed flames. This picometer-resolution dual-comb spectroscopic system was developed by using a single erbium-doped fiber laser at 1.5 μm along with a multipass optical configuration for the enhanced absorption measurement. Because of the mutual coherence of the two comb pulse trains emitted from the same laser cavity, DCS could be performed without using any phase-locking systems. Absorption spectra of CH_4/O_2/air flames over the spectral range 6503 cm^{-1} – 6535 cm^{-1} were measured at different reactant flow rates and heights above the burner, showing a good agreement with the spectral simulation of high-temperature H_2O using the HITEMP database. A noise equivalent (1σ) absorption coefficient of 9.5×10^{-5} cm^{-1} was achieved using the current DCS system. Besides, the dual-comb measurement of a C_2H_4/air sooting flame was also performed at the equivalence ratio Φ = 2.94 and compared with the spectral simulation of high-temperature H_2O and C_2H_2. All the spectral data were retrieved by 1500 averages of interferograms to increase the spectral signal-to-noise ratio (SNR), but a single interferogram could be acquired at 0.83 ms using the current free-running dual-wavelength fiber laser.

ARTICLE HISTORY
Received 27 August 2020
Revised 8 January 2021
Accepted 18 January 2021

KEYWORDS
Combustion diagnostics; dual-comb spectroscopy; free-running fiber laser; laminar flame

Introduction

Laser-absorption spectroscopy (LAS) provides a non-intrusive method for *in situ*, rapid, and quantitative measurements of species concentration and temperature in combustion environments (Farooq, Jeffries, Hanson 2008; Hanson et al., 2014; Hanson, Spearrin, Goldenstein 2016). When a laser beam is transmitted through the combustion field, the measured fractional transmission is directly related to gas

CONTACT Wei Ren renwei@mae.cuhk.edu.hk Department of Mechanical and Automation Engineering, Shenzhen Research Institute, The Chinese University of Hong Kong, New Territories, Hong Kong SAR, China.

properties by the well-known Beer's law. By using tunable semiconductor lasers as the light sources, high-resolution molecular spectroscopy could be readily attained by scanning the injection current or temperature of the semiconductor laser across the target absorption line(s). In the past decade, tunable diode laser-absorption spectroscopy (TDLAS) has been widely used for combustion research in laboratory-scale combustion facilities (Cheong et al. 2018; Ma, Lau, Ren 2017; Qu et al. 2015), and in practical combustion systems (Lee et al. 2018; Qu et al. 2018; Sur et al. 2015). However, a single distributed feedback (DFB) laser only covers a few wavenumbers when tuning the injection current and laser temperature. Therefore, multiple lasers and photodetectors are required for multi-species or multi-parameter detection in combustion measurements, which significantly increases the system cost and complexity.

Broadband light sources like optical frequency combs (OFCs) are nowadays of extraordinary interest to researchers in many fields (Picqué and Hänsch 2019). In general, the OFC source is a special mode-locked laser that emits thousands of equidistant (separated by the pulse repetition frequency) narrow-linewidth (kHz) comb teeth (optical frequencies) over a broadband spectrum. Frequency comb spectroscopy is becoming an attractive candidate for optical sensing and spectroscopy as many absorption lines of different molecules could be measured simultaneously by OFCs with a high resolution over a broad spectral range (Cundiff and Ye 2003; Diddams, Hollberg, Mbele 2007; Udem, Holzwarth, Hänsch 2002). In particular, dual-comb spectroscopy (DCS) has become a powerful tool for high-resolution molecular spectroscopy by the use of two coherent OFCs (Abbas et al. 2019; Coddington, Newbury, Swann 2016; Fllinger et al., 2019; Nakajima, Hata, Minoshima 2019). As schematically shown in Figure 1, a pair of frequency combs is normally generated from two ultrafast mode-locked lasers, which are phase-locked but with a slight difference in their repetition frequencies (i.e., f_r and $f_r + \Delta f_r$, respectively);

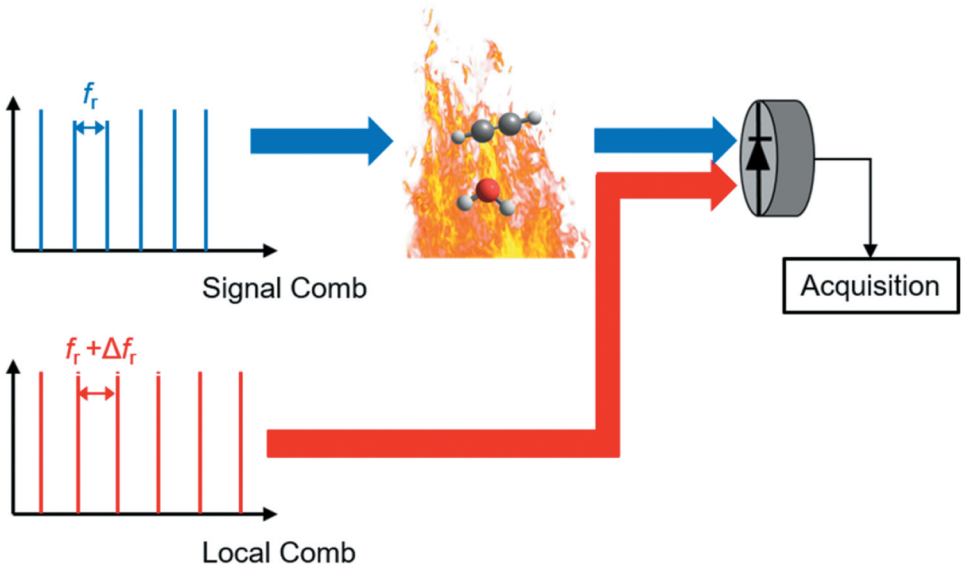

Figure 1. Schematic of dual-comb spectroscopy for combustion diagnostics.

here Δf_r is the frequency difference between the two combs. One of the OFCs (signal comb) passes through the gas medium and beats with the second comb (local comb) on a fast photodetector to generate a series of interferograms. Such an optical arrangement produces a radio frequency (RF) comb spectrum by the multi-heterodyne of adjacent comb teeth from these two OFCs. This method could be treated as an all-static spectroscopic method that performs Fourier-transform interferometry without any moving parts (Coddington, Newbury, Swann 2016).

Despite its evident spectroscopic advantages, only a few studies have been reported on the development of frequency comb spectroscopy for combustion diagnostics. The pioneering research was conducted by Foltynowicz's group and Rieker's group. Alrahman et al. (2014) reported the near-infrared cavity-enhanced optical frequency comb spectroscopy (CE-OFCS) in a premixed CH_4/air flat flame using an Er:fiber femtosecond laser and a fast-scanning Fourier-transform spectrometer. Based on the CE-OFCS method, the same group performed the sensitive detection of OH radical (Rutkowski et al. 2016) and studied the high-temperature water lines in the 6250–6670 cm^{-1} region (Rutkowski et al. 2018). Regarding the use of DCS for combustion research, Schroeder et al. (2017) demonstrated the first industrial application of a dual-comb spectrometer by measuring H_2O and CO_2 concentration transients in the exhaust of a 16 MW stationary natural gas turbine. Based on the same dual-comb sensor, Hayden et al. (2019) reported the detailed measurement of H_2O transitions from 1489.2 nm to 1492.5 nm at 2165 K. Additionally, Bergevin et al. (2018) applied the dual-comb spectroscopy to optically probe laser-induced plasmas. These groups conducted the breakthrough research of using DCS for combustion diagnostics. To our knowledge, we could hardly find any more research on using DCS for combustion diagnostics. Based on two independent mode-locked lasers, precise electronic feedbacks and complicated phase-locking systems are required to ensure the mutual coherence between the comb pair. Hence, it is of more interest to explore the possibility of performing sensitive and multi-species detection in combustion environments using low-cost and simple laser sources.

Coherent dual combs can be generated in a free-running dual-wavelength mode-locked fiber laser. Such a new lasing scheme was recently realized by Zhao et al. (2011) using a dual-wavelength passively mode-locked fiber laser. The dual-wavelength outputs come from a soliton erbium-doped fiber (EDF) laser which is passively mode-locked by a single-wall carbon nanotube saturable absorber (SWNT-SA). The gain profile of the EDF laser could be effectively controlled by adjusting the intracavity loss. The output comb teeth with a linewidth of ~250 Hz is spaced at a frequency difference Δf_r, which is determined by the intracavity group velocity dispersion. Hence, a simple and low-cost DCS system can be achieved with a single free-running fiber laser. Zhao et al. (2016) demonstrated picometer-resolution DCS of C_2H_2 near 1.5 μm with a spectral resolution of picometer using such a free-running dual-wavelength fiber laser. Xu et al. (2020) used a similar laser source and developed a dual-comb gas sensor for simultaneous C_2H_2 and NH_3 detection in a multipass gas cell at room temperature. The single-laser-based DCS was also extended to 1.8 μm – 2.0 μm for room-temperature H_2O detection using a thulium-doped mode-locked laser by Liao et al. (2018). To our knowledge, no research has been reported to make use of the free-running laser-based DCS system for combustion diagnostics.

In this paper, we report dual-comb spectroscopy for laminar premixed flames using a single free-running erbium-doped fiber laser. The dual-comb fiber laser covers the wavelength range 1530 nm – 1550 nm, where H_2O and C_2H_2 have many absorption lines under combustion environments. Real-time DCS flame measurements are achieved with a synchronized acquisition technique. Additionally, computational fluid dynamics (CFD) calculations are performed in this work to interpret the experimental data obtained in both CH_4/O_2/air non-sooting flames and C_2H_4/air sooting flames.

Experimental

Optical setup

The schematic of DCS used in this study for flame measurements is depicted in Figure 2. The dual-wavelength laser source shown in Figure 2(b) consists of a single fiber cavity formed by a 0.4-m erbium-doped fiber and a 3.2-m single-mode fiber, which is mode-locked by a single-wall carbon nanotube saturable absorber (SWNT-SA) (Xu et al. 2020). With the EDF-ring pumped by a 980-nm CW diode laser (LC96Z400, II–VI, USA), a unidirectional oscillation of pulses was produced inside the fiber cavity. A polarization controller (PC) was used to control the intracavity birefringence and polarization-

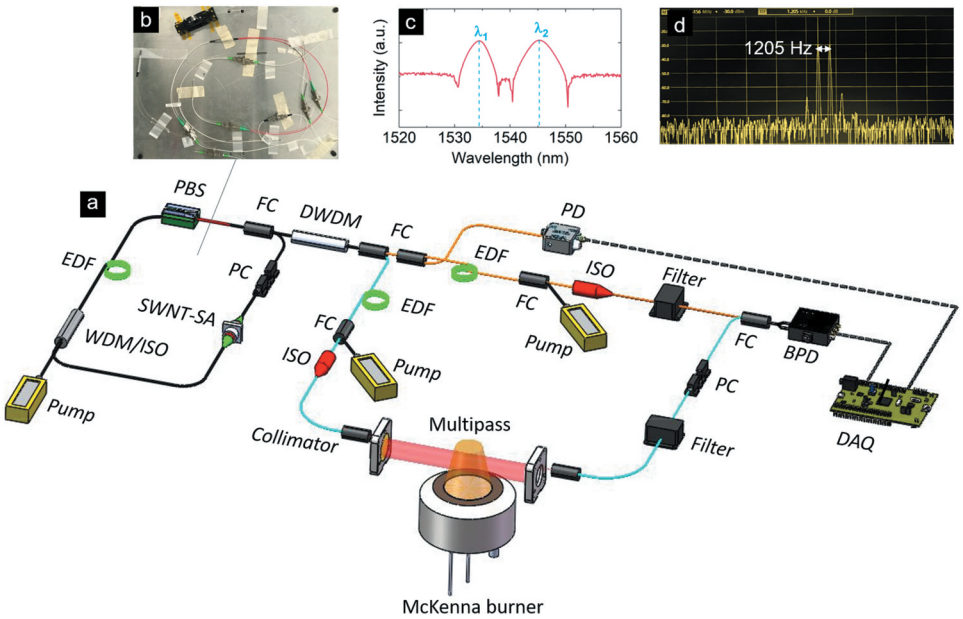

Figure 2. (a) Schematic of DCS for flame measurements using a single free-running mode-locked fiber laser. SWNT-SA, single-wall nanotube saturable absorber; WDM/ISO, wavelength division multiplexing/isolator; EDF, erbium-doped fiber; PBS, polarization beam splitter; PMF, polarization-maintaining fiber; FC, fiber coupler; PC, polarization controller; DWDM: dense wavelength division multiplexing; PD: photodetector; BPD: balanced photodetector; DAQ: data acquisition card. (b) Photograph of the dual-wavelength fiber laser source. (c) Optical spectrum of the laser output. (d) Measured laser repetition rates with a difference of 1205 Hz.

dependent loss. Thus, the dual-wavelength oscillation is generated when the fiber cavity is pumped above the mode-locking threshold. A polarization beam splitter (PBS) was used to ensure the polarization state. As illustrated in Figure 2(c), two output center wavelengths λ_1 (1534 nm) and λ_2 (1545 nm) were observed with a typical 3-dB spectral bandwidth of ~5 nm. The repetition frequencies of the comb outputs were measured to be 61156156 Hz and 61157361 Hz, respectively, resulting in a frequency difference Δf_r of 1205 Hz shown in Figure 2(d). The Δf_r was kept almost unchanged (standard deviation <20 mHz) over a test time of 10 minutes.

A two-stage dense wavelength division multiplexer (DWDM) divides the generated two pulse trains to form an optical interferometer. The pulse in each arm was further amplified with an EDF amplifier to achieve a broadened spectrum caused by strong nonlinear effects. We obtained a spectral overlap of ~20 nm between 1530 nm and 1550 nm in this work. Additionally, a tunable bandpass filter (TF1550-3.2, Dicon, USA) was used in the optical setup to prevent the possible aliasing issue.

As illustrated in Figure 2(a), the 1534-nm pulse was collimated to pass through the laminar flame stabilized on a McKenna burner. To increase the detection sensitivity, the burner was placed at the center of an open-path multipass configuration that is composed of two concave mirrors. A total of 19 optical passes were realized between these two mirrors. Considering the central porous plug with a diameter of 60 mm, we estimated an effective optical path length of 114 cm on the burner surface. The transmitted 1534-nm laser pulse was then coupled into a single-mode fiber and combined with the 1545-nm pulse to generate the time-domain interferogram. The power level was adjusted to be ~20 μW for both pulse trains to keep power balance and prevent nonlinear effects. Then, the generated interferograms were detected by a balanced photodetector (PDB425C, Thorlabs, USA). A synchronized acquisition technique was applied to achieve a fast interferogram acquisition with a limited on-board memory (Xu et al. 2020). As illustrated in Figure 2(a), a portion of the reference comb (1545 nm) was used as an external clock to trigger the high-speed data acquisition card. Hence, each interferogram was acquired at the acquisition time of $1/\Delta f_r$ (here 0.83 ms) and then Fourier-transformed to retrieve the spectral information.

Flame description

All the experiments were conducted for laminar premixed flames stabilized above a sintered stainless-steel porous disk with a diameter of 60 mm. The flame was shielded by nitrogen coming from the sintered bronze shroud ring to eliminate the ambient interference. The height of the burner surface relative to the optical table was

Table 1. Three representative reactant flow conditions used for CH_4/O_2/air premixed flames.

Gas supply	Flow rate A (L/min)	Flow rate B (L/min)	Flow rate C (L/min)
CH_4	1.2	1.2	1.0
O_2	1.6	1.9	1.9
Air	3.88	2.42	0.49

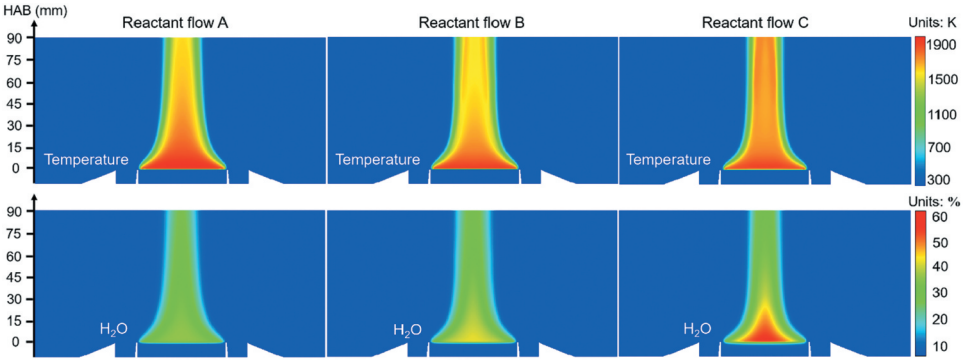

Figure 3. Simulated contours of flame temperature and H_2O concentration for the reactant flow conditions (A, B and C) listed in Table 1

adjustable so that the optical measurement could be conducted at different heights above the burner (HAB). We studied both the CH_4/O_2/air flames and the C_2H_4/air sooting flames in this work. The supplied CH_4, C_2H_4, air, O_2 and N_2 have purities of 99.99% (YaTai, China), 99.95% (YaTai, China), 99.99% (with H_2O < 20 ppm, Linde, Hong Kong SAR, China), 99.99% (Linde, Hong Kong SAR, China) and 99.999% (Linde, Hong Kong SAR, China), respectively. All the flow rates were monitored by the calibrated mass flow controllers (CS200, SevenStar, China) with an accuracy of ~1%. The equivalence ratio of the laminar premixed CH_4/O_2/air flame was fixed at $\Phi = 1$, and the flow rates of reactants were adjusted to obtain three representative flame conditions as summarized in Table 1. The flow rate of N_2 was fixed at 20 L/min.

To simulate all the flame conditions, the CFD calculations were performed using ANSYS Fluent. The flame structure can be reproduced using this comprehensive 2-D simulation, which includes buoyancy effects, radiative heat losses, and thermal diffusion. A reduced combustion mechanism DRM-22 of 24 species and 104 reactions was utilized in the CFD simulation (Kazakov and Frenklach, 1995). A pressure-based solver with coupled algorithms was used to solve the relevant governing equations of mass, momentum and energy. The second-order upwind scheme was used for the spatial discretization. Specific heat, viscosity, and thermal conductivity of the reactants were calculated using the ideal-gas-mixing law. The radiation was estimated using the discrete ordinate model, whereas the gas absorption coefficient was calculated using a weighted-sum-of-gray-gas model. Besides, temperature and velocity in downstream were also monitored as a reference for the determination of convergence. Based on the CFD model, Figure 3 presents the distributions of temperature and H_2O concentration for different reactant flow rates. The central flame temperature was also confirmed by a fine gage B-type (platinum-30% rhodium/platinum-6% rhodium) thermocouple (XMO, Omega, USA) with a deviation <1.5%; and more details of the thermocouple measurement could be found in our previous study (Ma et al. 2020; Ma, Lau, Ren 2017; Ma et al. 2018).

Additionally, C_2H_4 has been picked as the fuel for the standard ISF-4 premixed sooting flame by International Sooting Flame (ISF) Workshop (2020) and the well-known counterflow diffusion flame (Wang and Chung 2016). To stabilize the sooting flame, a stainless-steel porous disk was placed downstream ~30 mm above the burner.

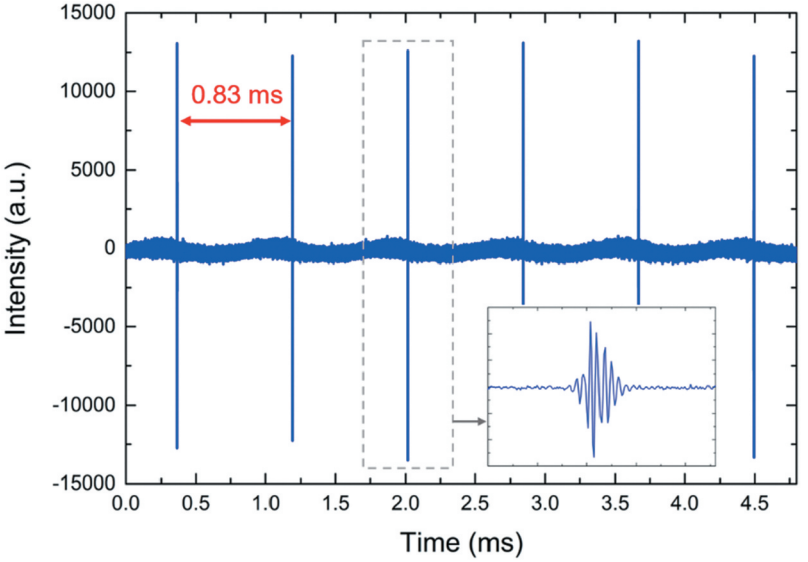

Figure 4. Representative interferograms acquired during the flame measurement. Inset: the interferogram with abscissa expanded 2000 times.

In this work, the flame was maintained at a fixed equivalence ratio $\Phi = 2.94$; the flow rate of N_2 co-flow was fixed at 10 L/min; and the flow rates of C_2H_4 and air were determined to be 1.6 L/min and 9.8 L/min, respectively. The central flame temperature was determined to be 1500 K at the HAB of 8 mm, and the H_2O and C_2H_2 concentrations were 8.8% and 3%, respectively.

Results and discussion

Time-domain interferogram acquisition

Figure 4 depicts the representative time-domain interferograms acquired in the CH_4/O_2/air premixed flame at the HAB of 8 mm. The inset graph demonstrates a typical beatnote signal. The interferograms show a constant interval of 0.83 ms, corresponding to the repetition frequency difference. The slight variation of the amplitude among the acquired interferograms may affect the background noise of the Fourier-transform spectrum.

Although a smaller variation of the interferogram amplitude is preferred, the acquired interferogram series may be disturbed by the unstable flow at a larger HAB. Figure 5 depicts the time-domain interferograms acquired at three different HABs of 8 mm, 15 mm and 20 mm. All the measurements were performed for the CH_4/O_2/air flame under the flow condition B listed in Table 1. The peak position of each interferogram is highlighted by the red circle shown in the figure. It is evident that the peak height varies more significantly when the HAB increases from 8 mm to 20 mm, which is mainly caused by the flame tip flickering above the burner. At the HAB of 8 mm and 15 mm, the periodic beatnote signal could be extracted clearly despite a certain variation of the background.

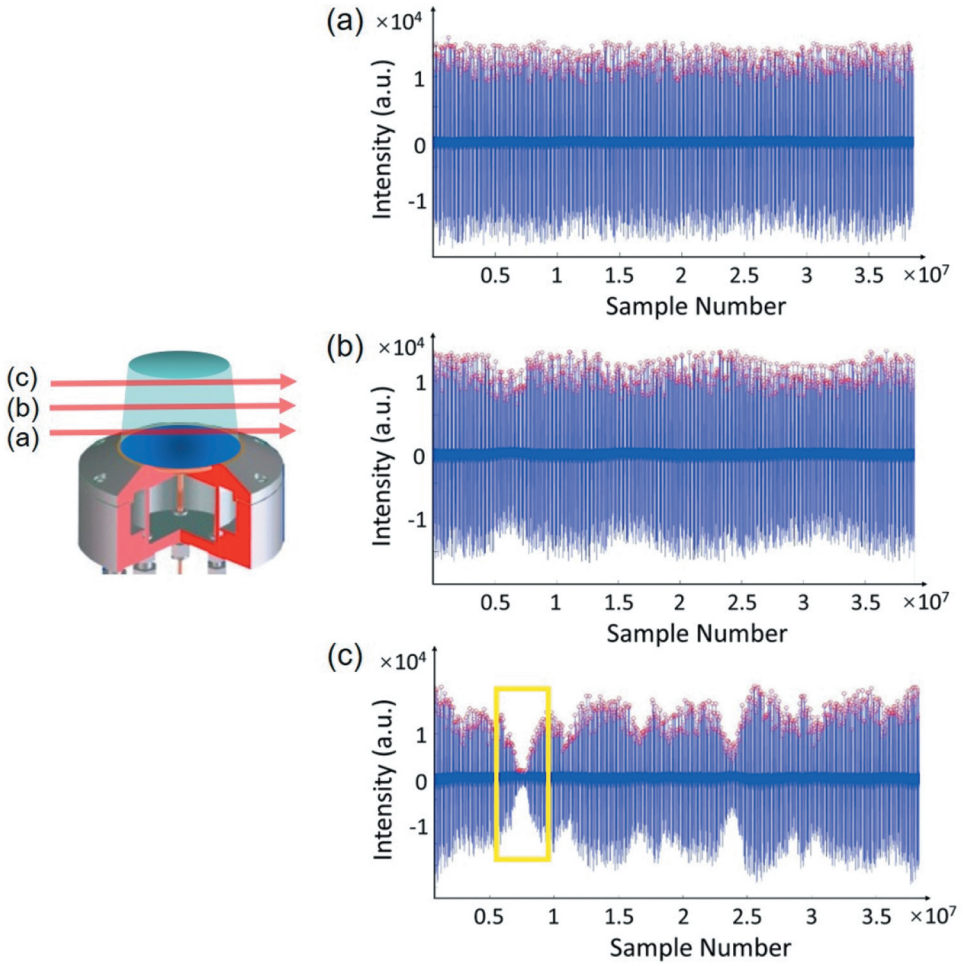

Figure 5. Influence of flame stability on the time-domain interferograms acquired at different HABs of the CH_4/O_2/air flame: (a) HAB = 8 mm, (b) HAB = 15 mm, and (c) HAB = 20 mm.

However, at the HAB of 20 mm, the interferograms particularly marked in the yellow window can be hardly distinguished from the background noise. Hence, in this work, we mainly focused on the dual-comb measurements at the HAB of 8 mm and 15 mm where the flame was relatively stable.

Spectral signal-to-noise ratio

The spectral averaging process is normally required in DCS to obtain a sufficient signal-to-noise ratio (SNR, defined as the ratio of the averaged magnitude of the spectral curve to the standard deviation of the baseline fluctuation) if the gas absorption is relatively weak. We first investigated the spectral SNR by measuring the CH_4/O_2/air flame under the stoichiometric condition (equivalence ratio $\Phi = 1$, flow rates: CH_4, 1.2 L/min; O_2, 1.6 L/min; air, 3.88 L/min) at the HAB of 8 mm. As shown in Figure 6, the SNR of the Fourier-transformed spectrum over the selected wavelength range (6520 cm^{-1} – 6540 cm^{-1}) increases with the

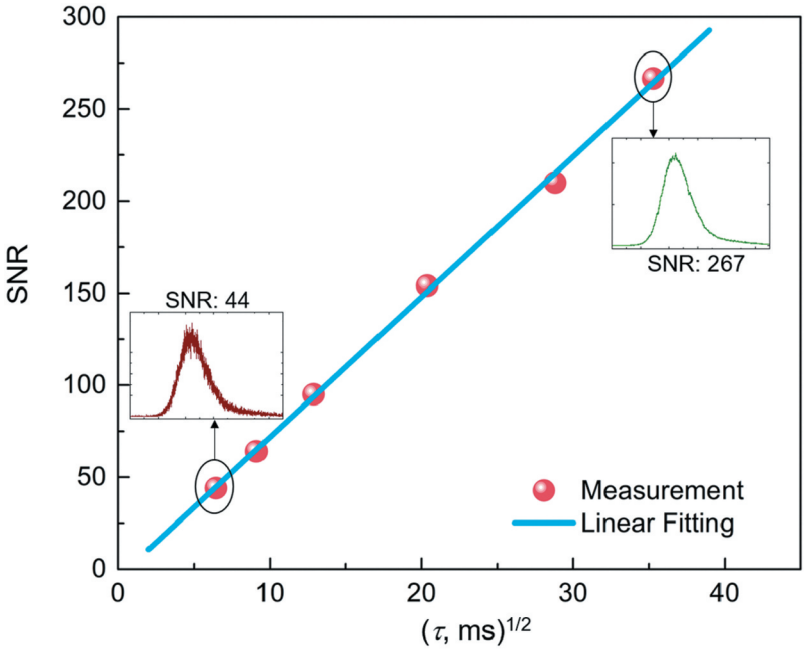

Figure 6. Variation of the spectral SNR with the interferogram acquisition time (τ, ms). The SNR increases linearly with the square root of τ.

acquisition time (τ). For instance, the absorption spectrum retrieved from 41.5 ms (50 interferograms) acquisition achieves an SNR of 44, which is increased to 267 at the acquisition time of 1245 ms (1500 interferograms).

An absorption-free baseline is required to determine the absorbance based on Beer's law. For the *in situ* flame measurement, we retrieved the spectral baseline by fitting the non-absorbing spectral region with the shape approximation of the optical bandpass filter used in the setup (Xu et al. 2020). As our dual-comb source was not locked to any reference optical frequency, the absolute frequency of each comb line is unknown. Hence, a priori knowledge of the spectral range determined by the bandpass filter and the line-center positions from the HITEMP database (Rothman et al. 2010) was needed for frequency calibration in actual flame measurements.

Flame measurement

Figure 7 presents the measured high-temperature absorption spectra of H_2O at the HAB of 8 mm in CH_4/O_2/air laminar flames (equivalence ratio $\Phi = 1$) with different reactant flow rates. Each spectrum was obtained by 1500 averages over the frequency range 6505 cm^{-1} – 6533 cm^{-1}. Under such non-sooting flame conditions, the absorption of H_2O dominates this particular spectral range compared to other species (i.e., C_2H_2) existing in the flame. Figure 7(a) illustrates the dual-comb measurement of the flame sustained at the flow condition A listed in Table 1, along with the spectral simulation of 35.9% H_2O at 1699 K based on the HITEMP database (Rothman et al. 2010). Here the species concentration was

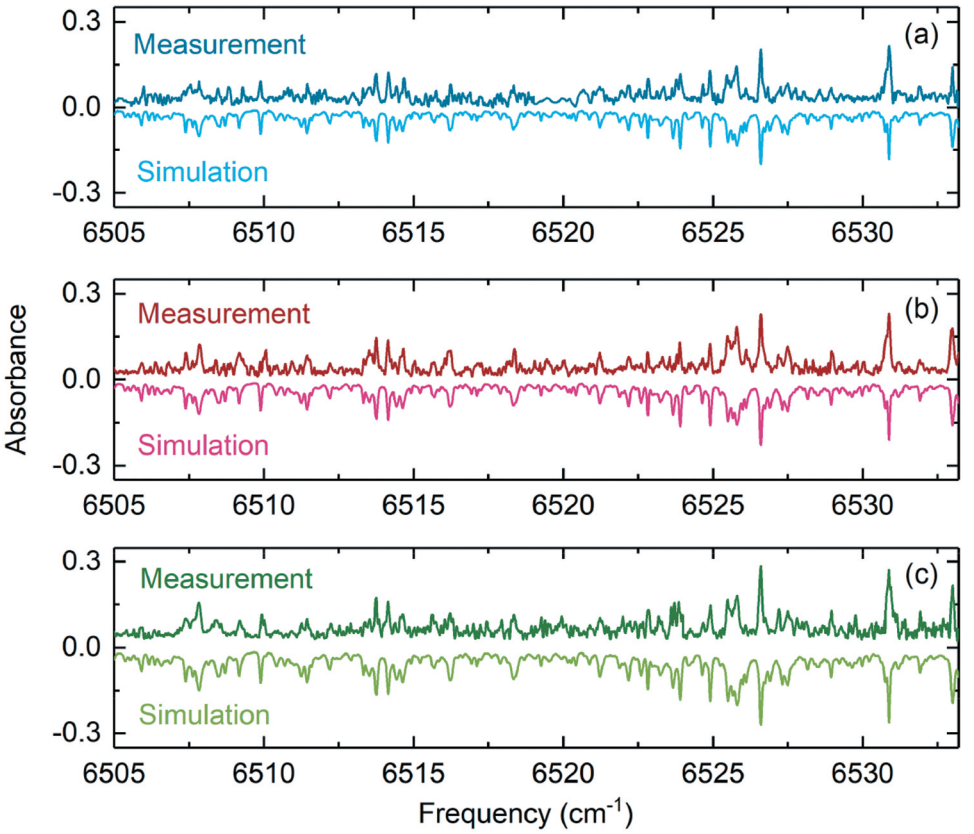

Figure 7. Comparison of the DCS measurements in CH_4/O_2/air laminar premixed flames with the spectral simulation of H_2O based on the HITEMP database (inverted for clarity). Both the experiment and simulation are at the HAB = 8 mm for three reactant flow conditions: (a) 1.2 L/min CH_4, 1.6 L/min O_2 and 3.88 L/min air; (b) 1.2 L/min CH_4, 1.9 L/min O_2, 2.42 L/min air; and (c) 1 L/min CH_4, 1.9 L/min O_2, 0.49 L/min air.

taken from the CFD simulation, and the central flame temperature was determined by the CFD simulation and confirmed by the thermocouple measurement. A relatively good agreement is found between the measurement and the simulation, particularly for the peak values. According to the effective path length of 114 cm and standard deviation of measurement noise (1σ), the noise equivalent absorption coefficient is determined to be 9.5×10^{-5} cm^{-1}. Figure 7(b) compares the measured and simulated spectra of H_2O at the flow condition B listed in Table 1, which provides a similar flame temperature of 1690 K and a slightly higher H_2O concentration of 43.4% compared to the flow condition A. Under the flame condition C listed in Table 1, the measured DCS of the flame at a lower temperature (1638 K) and higher H_2O concentration (58.5%) is plotted in Figure 7(c). Again the HITEMP simulation is in good agreement with the measurement. Besides, we compared the measurement with the spectral simulation for all the absorption lines with the peak absorbance above 0.04. It should be noted that the background noise is mainly caused by the carrier phase noise and the relative timing noise of the free-running fiber laser (Coddington, Newbury, Swann 2016). The overall deviation of the peak absorbance between the

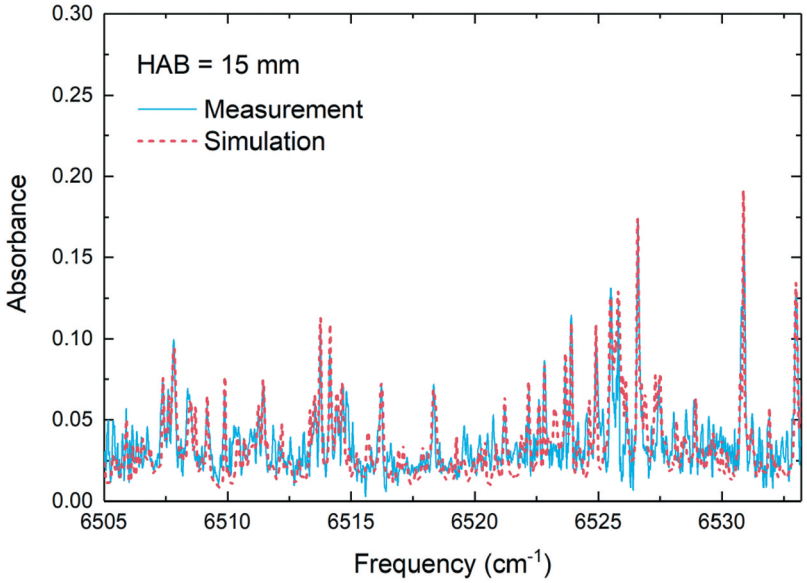

Figure 8. Comparison of the measured spectrum at HAB = 15 mm using DCS with the spectral simulation based on the HITEMP database. Reactant flow rates: 1.2 L/min CH_4, 1.9 L/min O_2, 2.42 L/min air.

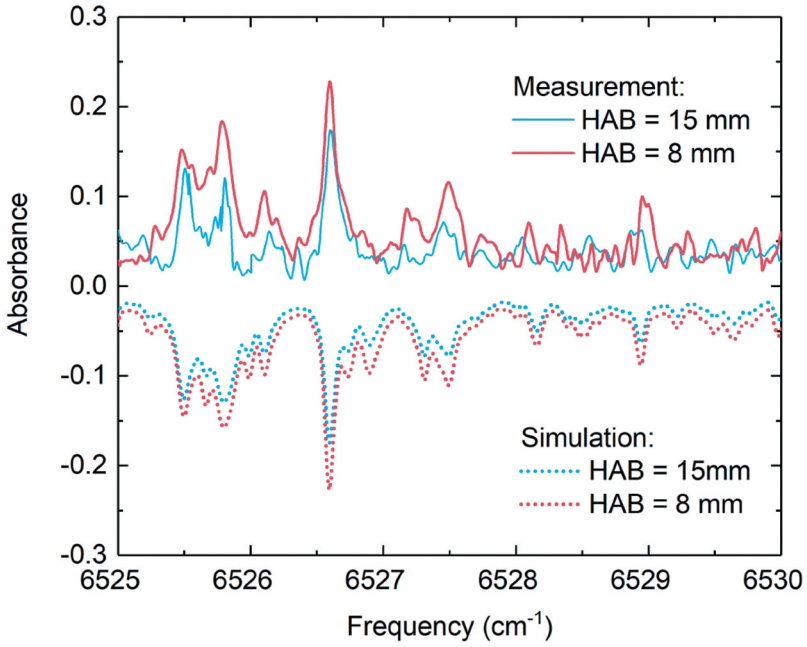

Figure 9. Comparison of the measured spectra of laminar flames (1.2 L/min CH_4, 1.9 L/min O_2, 2.42 L/min air) with the spectral simulations at two different HABs (8 mm and 15 mm), inverted for clarity.

measurement and simulation is determined to be 4.6%, 5.0% and 4.9%, respectively, for the three flame conditions.

Figure 8 presents the measured absorption spectrum (condition B listed in Table 1) at another HAB of 15 mm in the flame, along with the spectral simulation of H_2O using the HITEMP database. According to the CFD simulation shown in Figure 3, although the H_2O concentration keeps almost unchanged (43.4%) at a larger HAB, the hot core region of the flame is reduced with the increasing HAB. Hence, we used a shorter optical path (100 cm) and lower flame temperature 1550 K, both determined by the CFD simulation shown in Figure 3, for the spectral calculation illustrated in Figure 8. Despite the background noise in the measurement, a good agreement is seen between the measurement and the HITEMP simulation.

Figure 9 compares the DCS measurements at two different HABs (8 mm and 15 mm) of the laminar flame (flow condition B listed in Table 1). We only illustrate the spectral window between 6525 cm^{-1} and 6530 cm^{-1} for a clear comparison. The measurement captures the evident variation of the H_2O spectrum when the HAB changes from 8 mm to 15 mm, which is mainly caused by the variation of flame temperature. Although a relatively good agreement can be found between the measurement and spectral simulation for the strong absorption features, several weaker absorption lines, i.e., with the peak absorbance <0.04, cannot be distinguished from the background noise. It is possible to further improve the SNR by implementing more spectral averages but with a sacrifice of measurement time.

Finally, we performed the DCS of H_2O and C_2H_2 in a laminar C_2H_4/air premixed sooting flame at the equivalence ratio $\Phi = 2.94$ (reactant flow rates: 2.68 L/min C_2H_4 and

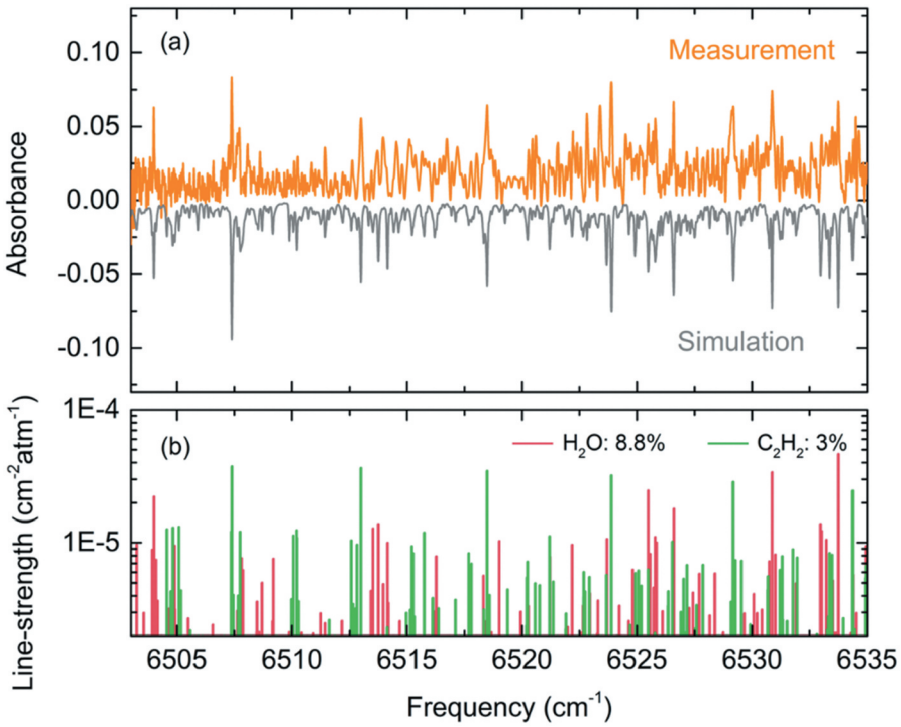

Figure 10. (a) Comparison of the measured and simulated absorption spectra of H_2O and C_2H_2 in a laminar C_2H_4/air sooting flame at the HAB of 8 mm. (b) Individual line-strengths of 8.8% H_2O and 3% C_2H_2 at 1500 K.

9.75 L/min air). Under such a typical sooting flame condition, the H_2O concentration is reduced to 8.8% at 1500 K but the C_2H_2 concentration is predicted to be 3%, which are probably detectable by the current dual-comb system. The measurement was conducted at the HAB of 8 mm. Figure 10(a) presents the measured absorption spectrum of the sooting flame along with the simulation of high-temperature H_2O and C_2H_2 using the HITEMP (Rothman et al. 2010) and HITRAN (Gordon et al. 2017) databases. Note that the spectroscopic parameters of C_2H_2 are only available in the HITRAN database. Despite the lower detection SNR (the peak absorbance is mostly below 0.1), a relatively good agreement is still observed between the DCS measurement and the spectral simulation. The individual absorption lines of H_2O and C_2H_2 are plotted in Figure 10(b) to identify the corresponding absorption features. The strong C_2H_2 and H_2O absorption lines (absorbance >0.04) can be clearly distinguished in the spectral range from 6503 cm^{-1} to 6535 cm^{-1}. It is promising to further enhance the detection limit by using a longer multipass configuration or an optical cavity (Alrahman et al. 2014; Wang et al. 2019); and it is also possible to investigate new methods such as the phase correction method to reduce the background noise.

Conclusions

In conclusion, we reported the dual-comb spectroscopy of H_2O and C_2H_2 in laminar premixed flames using a single free-running erbium-doped fiber laser. The laser source takes advantage of the mutual coherence of the two comb pulse trains emitted from the same laser cavity without using any phase-locking systems. We demonstrated the diagnostic capability of the current DCS system by measuring CH_4/O_2/air and C_2H_2/air flames at different flame conditions and heights above the burner. All the absorption spectra of the laminar flames were measured over the spectral range 6503 cm^{-1} – 6535 cm^{-1} and were retrieved by 1500 averages of the acquired interferograms at a time resolution of ~1.2 s. The detection accuracy was also demonstrated by comparing the measurement to the spectral simulation using the HITEMP and HITRAN databases. It is admitted that the measurement precision of the free-running fiber laser-based dual-comb system is not comparable to the highly stabilized DCS with phase-locked OFCs. However, the current precision of our system is sufficient for many combustion applications where the absorption features are broadened (normally gas pressure >1 bar). More importantly, our system is more suitable for practical applications such as combustion measurements due to the advantages of a simpler setup and no need for precise electronic feedbacks and complicated phase-locking systems.

It should be noted that DCS for combustion diagnostics is a typical line-of-sight measurement just like TDLAS. Hence, this technique must be combined with tomographic reconstruction methods to obtain both time-resolved and spatially resolved measurements. As tomographic absorption spectroscopy has been demonstrated for many combustion studies (Cai and Kaminski, 2017), tomographic DCS can also be deployed to other combustion systems with more complicated flame structures such as turbulent flames. Considering its wider spectral coverage, we believe that DCS is more promising for tomographic measurements compared to TDLAS. Additionally, the current DCS can be extended to other spectral ranges by using other doped fiber materials or

nonlinear fiber broadening methods. Future work is also planned to investigate the methods of improving the detection sensitivity by using a high-finesse optical cavity.

Nomenclature

LAS	Laser absorption spectroscopy
TDLAS	Tunable diode laser absorption spectroscopy
DFB	Distributed feedback
OFC	Optical frequency comb
DCS	Dual-comb spectroscopy
CE-OFCS	Cavity-enhanced optical frequency comb spectroscopy
f_r	Repetition frequency (Hz)
Δf_r	Repetition frequency difference (Hz)
EDF	Erbium-doped fiber
SWNT-SA	Single-wall carbon nanotube saturable absorber
CFD	Computational fluid dynamics
CW	Continuous wave
PC	Polarization controller
PBS	Polarization beam splitter
DWDM	Dense wavelength division multiplexing
Φ	Equivalence ratio
HAB	Height above the burner
SNR	Signal to noise ratio

Funding

This research is supported by the National Natural Science Foundation of China (NSFC) (51776179, 61435002, 61675014, 61675015), Research Grants Council of the Hong Kong SAR, China (14206317), and Open Research Fund from the State Key Laboratory of Applied Optics, China (SKLAO-201901).

References

Abbas, M. A., Q. Pan, J. Mandon, S. M. Cristescu, F. J. M. Harren, and A. Khodabakhsh 2019. Time-resolved mid-infrared dual-comb spectroscopy. Sci. Reports 9, 17247–55.

Alrahman, C. A., A. Khodabakhsh, F. M. Schmidt, Z. Qu, and A. Foltynowicz. 2014. Cavity-enhanced optical frequency comb spectroscopy of high-temperature H_2O in a flame. *Opt. Express* 22:13889–95. doi:10.1364/OE.22.013889.

Bergevin, J., T. Wu, J. Yeak, B. E. Brumfield, S. S. Harilal, M. C. Phillips, and R. J. Jones. 2018. Dual-comb spectroscopy of laser-induced plasmas. *Nat. Comm.* 9:1273–78. doi:10.1038/s41467-018-03703-0.

Cai, W., and C. F. Kaminski. 2017. Tomographic absorption spectroscopy for the study of gas dynamics and reactive flows. *Prog. Energy Combust. Sci.* 59:1–31.

Cheong, K.-P., L. H. Ma, Z. Wang, and W. Ren. 2018. Influence of line pair selection on flame tomography using infrared absorption spectroscopy. *Appl. Spectrosc.* 73 (5):529–39. doi:10.1177/0003702818815181.

Coddington, I., N. Newbury, and W. Swann. 2016. Dual-comb spectroscopy. *Optica* 3 (4):414–26. doi:10.1364/OPTICA.3.000414.

Cundiff, S. T., and J. Ye. 2003. Colloquium: Femtosecond optical frequency combs. *Rev. Mod. Phys.* 75 (1):325–42. doi:10.1103/RevModPhys.75.325.

Diddams, S. A., L. Hollberg, and V. Mbele. 2007. Molecular fingerprinting with the resolved modes of a femtosecond laser frequency comb. *Nature* 445 (7128):627–30. doi:10.1038/nature05524.

Farooq, A., J. B. Jeffries, and R. K. Hanson. 2008. In situ combustion measurements of H_2O and temperature near 2.5 μm using tunable diode laser absorption. *Meas. Sci. Technol.* 19 (7):075604. doi:10.1088/0957-0233/19/7/075604.

Fellinger, J., A. S. Mayer, G. Winkler, W. Grosinger, G. Truong, S. Droste, C. Li, C. M. Heyl, I. Hartl, and O. H. Heckl. 2019. Tunable dual-comb from an all-polarization maintaining single-cavity dual-color Yb:fiber laser. *Opt. Express* 27:28062–74. doi:10.1364/OE.27.028062.

Gordon, I. E., L. S. Rothman, C. Hill, R. V. Kochanov, Y. Tan, P. F. Bernath, M. Birk, V. Boudon, A. Campargue, K. V. Chance, et al. 2017. The HITRAN2016 molecular spectroscopic database. *J. Quant. Spectrosc. Radiat. Transf.* 203:3–69.

Hanson, R. K., and D. F. Davidson. 2014. Recent advances in laser absorption and shock tube methods for studies of combustion chemistry. *Prog. Energy Combust. Sci.* 44:103–14. doi:10.1016/j.pecs.2014.05.001.

Hanson, R. K., R. M. Spearrin, and C. S. Goldenstein. 2016. *Spectroscopy and optical diagnostics for gases*. Germany: Springer.

Hayden, T. R. S., N. Malarich, D. Petrykowski, S. P. Nigam, J. D. Christopher, C. Lapointe, N. T. Wimer, P. E. Hamlington, and G. B. Rieker. 2019. OH radical measurements in combustion environments using wavelength modulation spectroscopy and dual-frequency comb spectroscopy near 1491 nm. *Appl. Phys. B: Lasers Opt.* 125: doi: 10.1007/s00340-019-7341-6.

International Sooting Flame (ISF) Workshop. 2020. https://www.adelaide.edu.au/cet/isfworkshop/.

Kazakov, A., and M. Frenklach. 1995. http://combustion.berkeley.edu/drm/.

Lee, D. D., F. A. Bendana, S. A. Schumaker, and R. M. Spearrin. 2018. Wavelength modulation spectroscopy near 5 μm for carbon monoxide sensing in a high-pressure kerosene-fueled liquid rocket combustor. *Appl. Phys. B: Lasers Opt.* 124 (5):77. doi:10.1007/s00340-018-6945-6.

Liao, R., Y. Song, W. Liu, H. Shi, L. Chai, and M. Hu. 2018. Dual-comb spectroscopy with a single free-running thulium-doped fiber laser. *Opt. Express* 26 (8):11046–54. doi:10.1364/OE.26.011046.

Ma, L., H. Ning, J. Wu, and W. Ren. 2018. In situ flame temperature measurements using a mid-infrared two-line H_2O laser-absorption thermometry. *Combust. Sci. Technol.* 190 (3):393–408. doi:10.1080/00102202.2017.1392515.

Ma, L., K.-P. Cheong, H. Ning, and W. Ren. 2020. An improved study of the uniformity of laminar premixed flames using laser absorption spectroscopy and CFD simulation. *Exp. Therm. Fluid Sci.* 112:110013. doi:10.1016/j.expthermflusci.2019.110013.

Ma, L. H., L. Y. Lau, and W. Ren. 2017. Non-uniform temperature and species concentration measurements in a laminar flame using multiband infrared absorption spectroscopy. *Appl. Phys. B: Lasers Opt.* 123 (3):83. doi:10.1007/s00340-017-6645-7.

Nakajima, Y., Y. Hata, and K. Minoshima. 2019. High-coherence ultra-broadband bidirectional dual-comb fiber laser. *Opt. Express* 27:5931. doi:10.1364/OE.27.005931.

Picqué, N., and T. W. Hänsch. 2019. Frequency comb spectroscopy. *Nat. Photonics* 13:146–57. doi:10.1038/s41566-018-0347-5.

Qu, Z., P. Holmgren, N. Skoglund, D. R. Wagner, M. Broström, and F. M. Schmidt. 2018. Distribution of temperature, H_2O and atomic potassium during entrained flow biomass combustion–Coupling in situ TDLAS with modeling approaches and ash chemistry. *Combust. Flame* 188:488–97. doi:10.1016/j.combustflame.2017.10.013.

Qu, Z., R. Ghorbani, D. Valiev, and F. M. Schmidt. 2015. Calibration-free scanned wavelength modulation spectroscopy–application to H_2O and temperature sensing in flames.. *Opt. Express* 23 (12):16492–99. doi:10.1364/OE.23.016492.

Rothman, L. S., I. E. Gordon, R. J. Barber, H. Dothe, R. R. Gamache, A. Goldman, V. I. Perevalov, S. A. Tashkun, and J. Tennyson. 2010. HITEMP, the high-temperature molecular spectroscopic database. *J. Quant. Spectrosc. Radiat. Transf.* 111:2139–50. doi:10.1016/j.jqsrt.2010.05.001.

Rutkowski, L., A. Foltynowicz, F. M. Schmidt, A. C. Johansson, A. Khodabakhsh, A. A. Kyuberis, N. F. Zobov, O. L. Polyansky, S. N. Yurchenko, and J. Tennyson. 2018. An experimental water line list at 1950 K in the 6250–6670 cm^{-1} region. *J. Quant. Spectrosc. Radiat. Transf.* 205:213–19. doi:10.1016/j.jqsrt.2017.10.016.

Rutkowski, L., A. C. Johansson, D. Valiev, A. Khodabakhsh, A. Tkacz, F. M. Schmidt, and A. Foltynowicz. 2016. Detection of OH in an atmospheric flame at 1.5 μm using optical frequency comb spectroscopy. *Phot. Lett. Of Poland* 8:110–12. doi:10.4302/plp.2016.4.07.

Schroeder, P. J., R. J. Wright, S. Coburn, B. Sodergren, K. C. Cossel, S. Droste, G. W. Truong, E. Baumann, F. R. Giorgetta, I. Coddington, et al. 2017. Dual frequency comb laser absorption spectroscopy in a 16 MW gas turbine exhaust. *Proc. Combust. Inst.* 36:4565–73. doi:10.1016/j.proci.2016.06.032.

Sur, R., K. Sun, J. B. Jeffries, J. G. Socha, and R. K. Hanson. 2015. Scanned-wavelength-modulation-spectroscopy sensor for CO, CO_2, CH_4 and H_2O in a high-pressure engineering-scale transport-reactor coal gasifier. *Fuel* 150:102–11. doi:10.1016/j.fuel.2015.02.003.

Udem, T., R. Holzwarth, and T. W. Hänsch. 2002. Optical frequency metrology. *Nature* 416 (6877):233–37. doi:10.1038/416233a.

Wang, Y., and S. H. Chung. 2016. Formation of soot in counterflow diffusion flames with carbon dioxide dilution. *Combust. Sci. Technol* 188 (4–5):805–17. doi:10.1080/00102202.2016.1139388.

Wang, Z., Q. Wang, W. Zhang, H. Wei, Y. Li, and W. Ren. 2019. Ultrasensitive photoacoustic detection in a high-finesse cavity with pound–drever–hall locking. *Opt. Lett.* 44 (8):1924–27. doi:10.1364/OL.44.001924.

Xu, K., X. Zhao, Z. Wang, J. Chen, T. Li, Z. Zheng, and W. Ren. 2020. Multipass-assisted dual-comb gas sensor for multi-species detection using a free-running fiber laser. *Appl. Phys. B: Lasers Opt.* 126:39. doi:10.1007/s00340-020-7382-x.

Zhao, X., G. Hu, B. Zhao, C. Li, Y. Pan, Y. Liu, T. Yasui, and Z. Zheng. 2016. Picometer-resolution dual-comb spectroscopy with a free-running fiber laser. *Opt. Express* 24 (19):21833–45. doi:10.1364/OE.24.021833.

Zhao, X., Z. Zheng, L. Liu, Y. Liu, Y. Jiang, X. Yang, and J. Zhu. 2011. Switchable, dual-wavelength passively mode-locked ultrafast fiber laser based on a single-wall carbon nanotube modelocker and intracavity loss tuning. *Opt. Express* 19 (2):1168–73. doi:10.1364/OE.19.001168.